

Design and Simulating an X-Band Light Weight Phase Array Antenna with Integrated Phase Shifter

Nima Beiranvand¹ and Mohammadreza Shahkhah^{*2}

Abstract- The advancement of technology has significantly increased the importance of defense systems that can scan and identify attacking targets. These systems rely on phased array antennas to achieve their functionality. The beam remains fixed in a perpendicular orientation without such antennas, preventing effective target detection. Historically, beam rotation was accomplished either mechanically or electronically. Mechanical methods involved the use of levers that required constant rotation, whereas electronic beam rotation was enabled solely by phased array antennas. This process necessitates the use of phase shifters, which are typically implemented using either pin diodes or ferrites. In this article, pin diodes are utilized due to their advantages, including high switching speed, reversibility, and superior availability compared to ferrites.

Rather than placing all the PIN diodes on a single unit and rotating the entire antenna pattern to the desired angle, this approach proves to be inefficient, as replacing the PIN diodes each time would be impractical. Additionally, constructing such a system would be highly complex. To address these challenges, a more efficient solution involves quantizing the PIN diode phases into two discrete states: 0° (off) and 180° (on), which are incorporated into a single-bit unit cell with dimensions of 7×7 . This configuration allows for the beam to be rotated to the desired angle while maintaining system simplicity. However, one important characteristic of this type of antenna is that, as the scanning coverage angle increases, the antenna gain decreases.

Index Terms -- Electronic beam steering, phased array antenna, phase shifters, diode pins, unit cell

I. INTRODUCTION

Radars utilize mechanical and electronic methods to cover their surrounding space. The slow speed and mechanical limitations are significant drawbacks of mechanical beam steering. Electronic beam steering offers a solution to overcome these deficiencies. However, it is essential to note that electronic methods incur higher costs than mechanical ones, as phase shifters replace mechanical levers for beam rotation. One advantage of electronic beam steering is the rapid rotation speed for target identification. This allows for adjustable beam angles and signal coverage. By appropriately setting the angle, the signal's radiation direction can be altered, and the coverage range can be adjusted[1]. Beam rotation allows the radiation pattern to change, enabling the beam to be emitted at various angles. Electronic beam steering is feasible only with transmitting and reflecting phased array antennas.

The demand for transmitting phased array antennas is increasing in telecommunications systems, radars, and satellite stations due to their ability to emit multiple beams when connected to phase shifter elements simultaneously. This is unlike microstrip antennas, which typically exhibit low gain and are commonly used in mobile phone systems[2].

As the number of phase shifter elements increases, more power is fed into the system, enhancing the radar range and gain.

Phase shifters can be classified into diode pins and ferrites; this paper focuses on diode pins.

Furthermore, diode pins act as low-resistance components at high frequencies, allowing current to flow rapidly without significant Voltage drop[3]. This paper concentrates on designing and simulating a transmitting phased array antenna, as outlined in Table I.

TABLE I

Amount	Parameters	row
45Degree	Total angle covered	1
$^\circ 18$	half power beam width	2
Less than 5°	Angle change step	3
linear	Polarization	4
Less than 1.5	Return Loss (VSWR)	5
1 kilogram	Total weight (antenna, control board, and feeding network)	6
15 cm \times 15 cm \times 10 mm	Dimensions	7
1 watt	Tolerable power	8
126mm	A(area)	9
35mm	Horn a	10
27mm	Horn b	11
2inch	horn flare length	12
3×10^8	C	13
9.5 G	Center frequency	14
$3 \times 10^8 / 9.5 = 31.5$	$\lambda = c/f$	15

A. Literature Review

The literature reveals a historical progression in beam steering methodologies. In 1996, Professor McManamon et al. [4]. Utilized mechanical methods in radar systems but concluded that the inherent limitations made these approaches unsuitable for practical beam guidance. By 2010, Montazeri et al. [5] developed a beam steering array within micro-electromechanical systems using single-bit phase shifters to determine scanned angles, demonstrating that increased phase shifter elements significantly enhanced system power, gain, and radar range. In 2011, Kamoda et al [6]. They have highlighted the advantages of larger antenna arrays for improving beam shaping and directionality through phase shifters. By 2014, Yaacobi et al. [7] illustrated that phased array systems could achieve beam rotation of up to 24 degrees, asserting that reflecting arrays fed spatially exhibit minimal losses when integrated with phase shifters. Clemente et al. [8]proposed a unit cell with a single-bit phase (0 or 180 degrees), simulated using U and O grooves in 2012. Their research indicated that quantizing phase shifts from one to two bits could lead to a gain reduction of up to 4 dB, with further increases in angle resulting in more pronounced gain

1. Imam Hossein University, Tehran, Iran.

* Corresponding author Email: rezashahkhah01@gmail.com

2. Islamic Azad University Tehran Branch, Tehran, Iran.

losses. Sboui et al. proposed a novel tunable frequency antenna, incorporating two varactor diodes. The antenna radiates through a U-groove on a hexagonal cavity, with the resonance frequency being adjustable by varying the capacitance of the varactor diodes[9]. Manoochehri et al. employed a conical crossover antenna design to enhance the beam width and observed that the incorporation of a surface reflector was considered as a means to mitigate the back radiation lobe[10]. Li and Zhao proposed a novel antenna patch element design aimed at extending the scanning range of phased array antennas. The structure incorporates a driving element and utilizes four p-i-n diodes, enabling beam reconfiguration and thereby expanding the scanning angle of the array[11]. In 2014, Ayach et al.[12] outlined design trends for phase shifters operating at 10 GHz, concluding that these shifters exhibit low losses while acknowledging that beam rotation may contribute to gain reduction. These studies indicate that fluctuations in gain with varying scan angles in phased array antennas represent a critical unresolved issue, with a significant degradation in gain persisting despite beam rotation [13].

The present research seeks to integrate a phased array antenna featuring multiple beam-steering elements to achieve higher rotation speeds than mechanical methods while addressing the substantial gain loss associated with the inverse relationship between half-power beam width and gain. Additionally, this study proposes an optimization strategy for diode pin adjustments during beam rotation to enhance overall system performance. Integrating antenna elements and phase shifters involves placing PIN diodes on the antenna components. In addition to radiating electromagnetic waves, these elements also serve as phase shifters and help mitigate gain loss during beam steering.

II. SIMULATION METHOD FOR SINGLE-BIT UNIT CELL

Fig. 1 illustrates the proposed unit cell. This cell features a rectangular section measuring 7.3 mm by 8.2 mm with an O-shaped groove on one side (Fig. 2) and a similarly sized piece with a U-shaped groove on the other (Fig. 3). Both pieces are connected by a metal hole, denoted as 'dv' in Fig. 1, with a diameter of 0.38 mm at their center. As shown in Fig. 1, the components are placed on two identical substrates. RO4003, $h=1.524\text{mm}$. These two substrates are separated by a copper ground plane with a thickness of 18 micrometers and are interconnected by the substrate. RO4403, $h_b=0.09\text{mm}$. The two substrates are separated by a ground plane made of copper with a thickness of 18 micrometers and are interconnected through the substrate. Two O-shaped pin diodes are integrated with the active component shown in Fig. 2. This component, similar to the passive component depicted in Fig. 3, is connected to a narrow bias line measuring 0.21 millimeters via a vertical connection of 0.15 millimeters. Depending on the bias current, the radiated field can rotate either 0° or 180° .

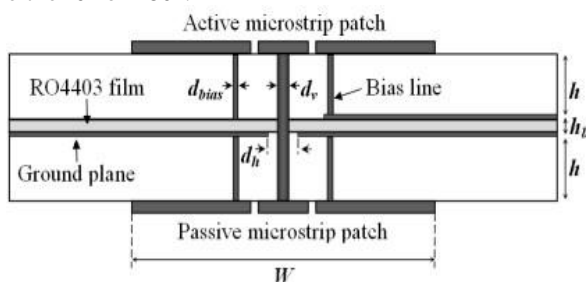


Fig. 1. Geometry of the unit cell[14]

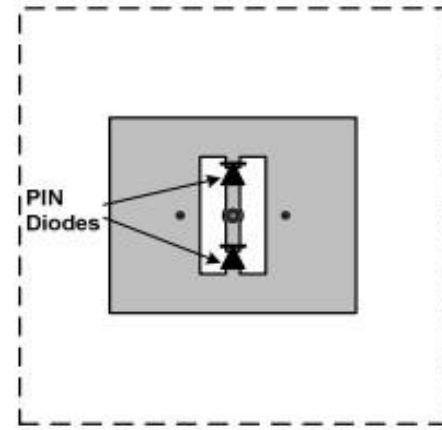


Fig. 2. O-shaped active component with two-pin diodes

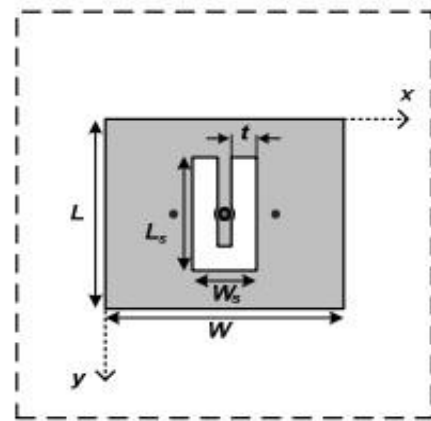


Fig. 3. U-shaped passive component

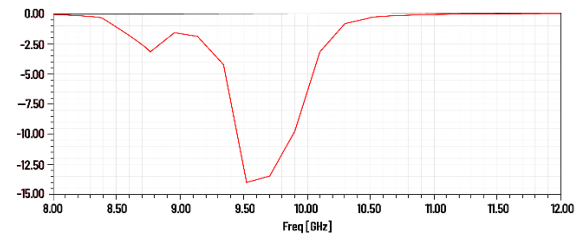


Fig. 4. Return losses of the pin diode in a single-bit unit cell in the ON state

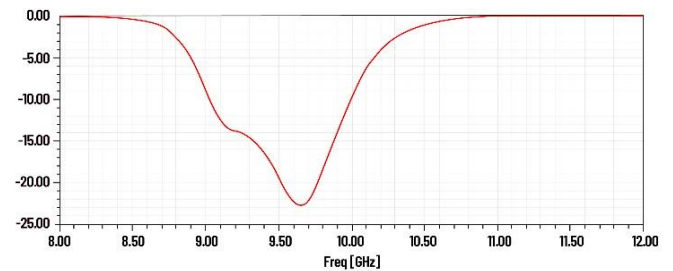


Fig. 5. Phase of the pin diode in a single-bit unit cell in the OFF state

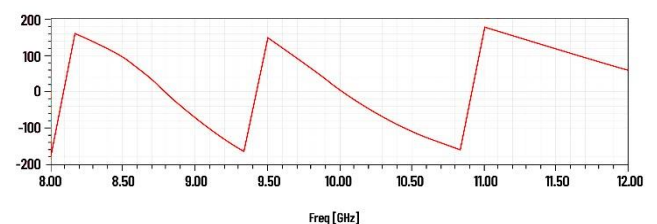


Fig. 6 - Phase of the pin diode in a single-bit unit cell in the ON state

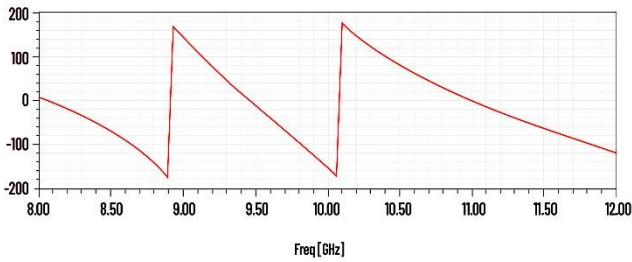


Fig. 7 - Phase of the pin diode in a single-bit unit cell in the OFF state

III. CALCULATION OF THE BEAM ROTATION FOR ARRAY ANTENNAS.

The beam steering or the distance between elements is calculated using (1),

$$d/\lambda \leq 1/(1 + \sin\theta) \quad (1)$$

Where(d) is the distance between elements, (λ) is the wavelength, and (θ) is the beam steering angle. For example, if the distance between elements is 23.5 millimeters and the wavelength is 31.57 millimeters, the maximum beam steering angle is 20°. The distance between elements must be reduced to increase the maximum beam steering angle at a constant wavelength. In the example mentioned earlier, if the distance between elements is 18 millimeters, the maximum beam steering angle becomes 48.5°.

B. Antenna Array

An antenna is responsible for radiating electromagnetic waves into free space. An antenna array is a collection of elements arranged together for a specific application. In this study, for the single-bit unit cell, the user-designed antenna array consists of a 7×7 element configuration with a center-to-center spacing of 18 millimeters for beam steering. Fig. 8 illustrates an overview of this antenna array within the simulation environment.

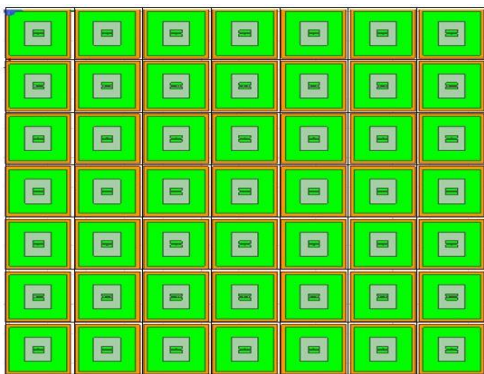


Fig. 8. Representation of the single-bit unit cell antenna array

C. Feed Network

In this paper, a pyramidal horn antenna is employed to feed a one-bit cell array, as illustrated in Fig. 9. This type of antenna is selected due to its capability to provide linear polarization. The design process encompasses two primary components. The first component is the waveguide, which is tailored according to the operating frequency. The focus of this study is on a central frequency of 9.5 GHz, which is situated within the X-band range. The second component is the horn aperture, designated as "horn a" and "horn b," where

'a' represents the aperture length and 'b' signifies the aperture width. To begin with, the dimensions of the horn aperture must be established, typically measured in millimeters or centimeters. The antenna is subsequently simulated using two distinct methods. The dimensions of the aperture (a,b), the focal distance (F), and other pertinent parameters and relationships are presented below. The wavelength, denoted as λ , is calculated using the formula: speed of light divided by frequency. The area of the array, represented by A, is established at 126 mm². The "horn flare length" pertains to the distance the waveguide must extend to connect to the aperture, which may, for example, be set to 2 inches; this parameter has a negligible impact on the simulation outcomes. The values of D and the far-field region are derived from equations (1), (2), and (3). [15]
 $a=35\text{mm}$, $b=27\text{mm}$, $\lambda=c/f=3\times 10^8/9.5=31.5$, $A=126\text{mm}$, horn flare length=2inch, $\Delta\theta=45^\circ$

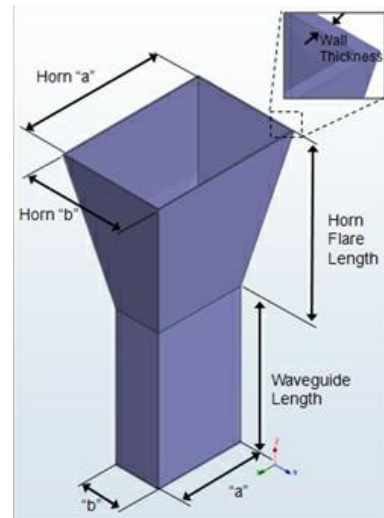


Fig. 9. illustrates the specifications of the pyramidal horn antenna.[16]

In the first method, the antenna is positioned in front of the phased array, and a simulation is performed. Then, the half-power beam width is calculated, and the sidelobe level is obtained at the desired tapering level. In the second method, the antenna is not placed in front of the phase-shifting elements. Instead, the simulation is carried out, and the maximum antenna gain is determined. The sidelobe level is then calculated by subtracting the maximum value, and $\Delta\theta$ is obtained. Finally, the value of F is calculated. If $F \geq \text{Far Field}$, it means we are in the far-field region. The selected dimensions are appropriate for use with this antenna. However, it is important to ensure that the condition $F \geq \text{Far Field}$ is satisfied. If the far-field distance exceeds the focal distance (F), the antenna dimensions must be re-evaluated and adjusted accordingly. Please modify the dimensions of the antenna until the specified condition is met. The waveguide that will ultimately be simulated will correspond to these revised dimensions.

$$F = \frac{A}{2 \times \tan\Delta\theta} \quad (1)$$

$$D = \sqrt{(\text{Horn}_a^2 + \text{Horn}_b^2)} \quad (2)$$

$$\text{FarField} = \frac{2D^2}{\lambda} \quad (3)$$

The chosen dimensions for the antenna are suitable; however, it is crucial to verify that the condition $F \geq \text{Far Field}$

is fulfilled. Should the far-field distance be greater than the focal distance (F), a re-evaluation and adjustment of the antenna dimensions will be necessary. Please make the necessary modifications to the antenna dimensions until this condition is achieved. The waveguide for the simulation will reflect these updated dimensions.

It should be noted that sometimes you find yourself at distances of 0.2 mm or 0.3 mm within the near-field area. For instance, at 0.3 mm, you could be as far as 3 mm away from the far-field region. This is due to the small dimensions of the antenna; regardless of how you modify the antenna's size, it won't transition into the far-field area, hence the simulation must continue. After adjusting, the value of D is obtained, which is 63 mm. The data yielded in the corresponding Fig. shows a value of $s_{1,1} = -20.4$, which is quite favorable, as it needs to be less than -10.

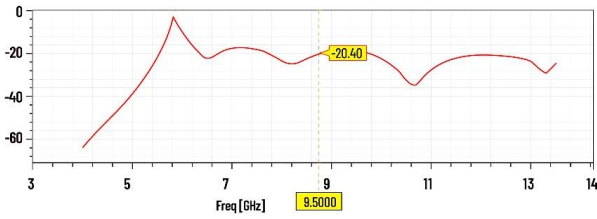


Fig. 10. illustrates the value of $s_{1,1}$

Then, we consider the realized gain, which is valued at 10.56. Following this, a phased array is to be positioned in front of the antenna. The tapering value of the array will then be calculated and subtracted from the realized gain.

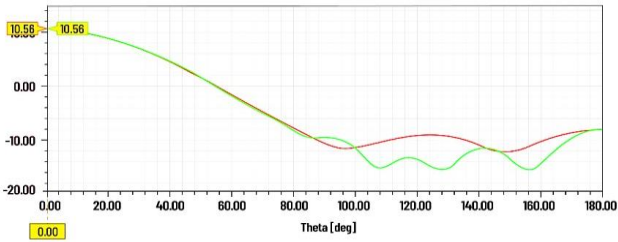


Fig. 11. illustrates the value of realized gain

IV. BEAM STEERING

Beam steering is achieved using the phase scanning method, which involves phase error and command. To calculate the phase error, as shown in Fig. 12, if a pyramidal horn antenna is positioned in front of the central element of a transmitting antenna array, it can be stated that the phase error of the central component is zero, and the exact phase of this element is derived from Equation (4).[15]

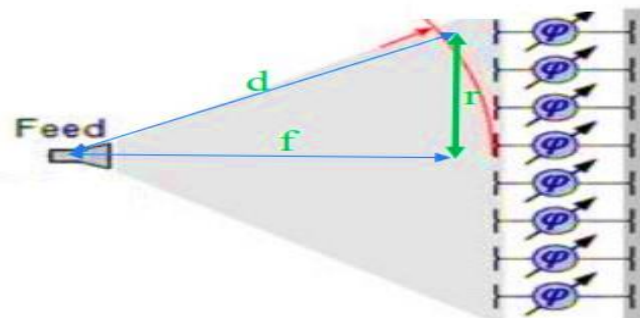


Fig. 12. The horn antenna is positioned before the phase-shifting elements.

However, other elements of the transmitting antenna array will have phase errors, which can also be calculated accurately from Equation (4).[15]

$$\phi_{center} = k_0 \times F, k_0 = \frac{2\pi}{\lambda} \quad (4)$$

$$\phi_{offset} = k_0 \times (\sqrt{(F \cdot 2 + (pox \cdot 2 + poy \cdot 2))}) - phi1 \quad (5)$$

In Equation (5),[15] each element's spatial position and the central component's initial phase are defined, and the phase command is assumed from Equation (6).[15] The array of elements is arranged as shown in Fig. 13, where the distance between elements and the phase shift of elements along the x-axis and the distance between elements and the phase shift of elements along the y-axis are discussed.[15]

$$\psi_x = kd_x \sin\theta \cos\phi + \beta_x \quad (6)$$

$$\psi_y = kd_y \sin\theta \sin\phi + \beta_y \quad (7)$$

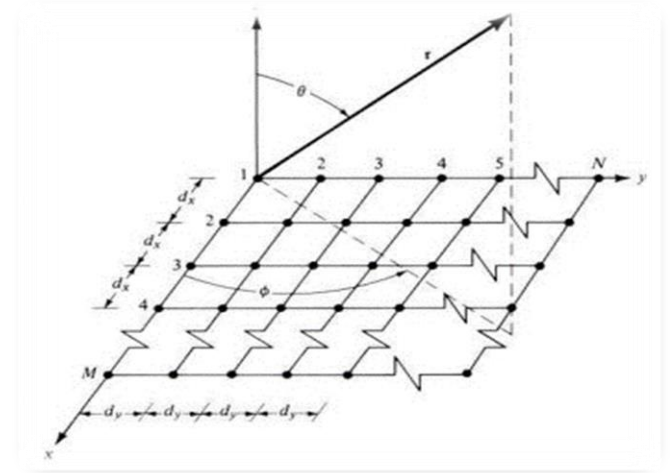


Fig. 13. Geometry of the planar arrays

If the objective is to have only one main beam in the direction of (b, v), the above equations can be rewritten as follows.[15]

$$\beta_x = -kd_x \sin\theta_0 \cos\phi_0 \quad (8)$$

$$\beta_y = -kd_y \sin\theta_0 \sin\phi_0 \quad (9)$$

Thus, the phase command is given by[15]:

$$\phi_{str} = \beta_x + \beta_y \quad (10)$$

In general, the beam steering in the phase scanning method is expressed as[15]:

$$\phi_{total} = \phi_{str} - \phi_{offset} \quad (11)$$

Beam Steering in the First State

Rotation of the Beam in the Initial State In this case[15], the arrangement of the elements is based on Equation (12)

$$\begin{aligned} \text{if } 0^\circ < \phi_{total} < 180^\circ &\Rightarrow \phi_{total} = 0^\circ \\ \text{if } 180^\circ \leq \phi_{total} \leq 360^\circ &\Rightarrow \phi_{total} = 180^\circ \end{aligned} \quad (12)$$

The outputs are represented in the following Figures.

V. BEAM STEERING

Beam Steering in the Second State. In this case, the arrangement of the elements is based on Equation (13).

$$\begin{cases} \text{if } 0^\circ \leq \phi_{total} < 90^\circ \Rightarrow \phi_{total} = 0^\circ \\ \text{if } 90^\circ \leq \phi_{total} \leq 270^\circ \Rightarrow \phi_{total} = 180^\circ \\ \text{if } 270^\circ < \phi_{total} \leq 360^\circ \Rightarrow \phi_{total} = 0^\circ \end{cases} \quad (13)$$

The outputs are represented in the following Figures.

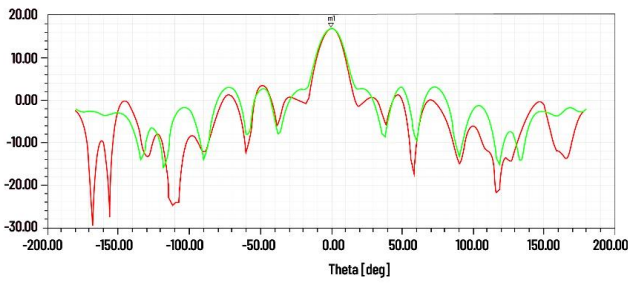


Fig. 14. Results of beam Rotation in the Initial State with. $\theta_{str} = 0^\circ$ and $\varphi_{str} = 0^\circ$ for Case One

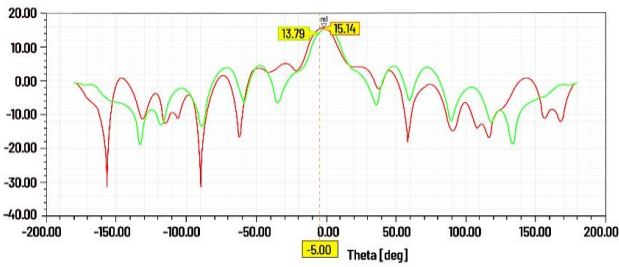


Fig. 15. Results of beam Rotation in the Initial State with. $\theta_{str} = -5^\circ$ and $\varphi_{str} = 0^\circ$ for Case One

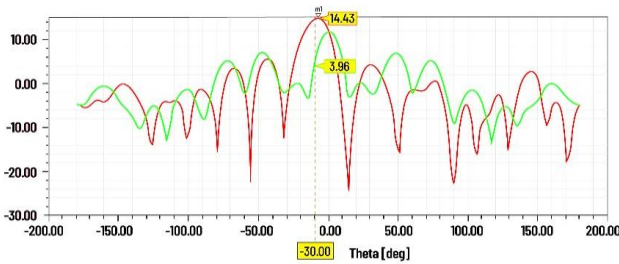


Fig. 16. Results of beam Rotation in the Initial State with. $\theta_{str} = -10^\circ$ and $\varphi_{str} = 0^\circ$ for Case One

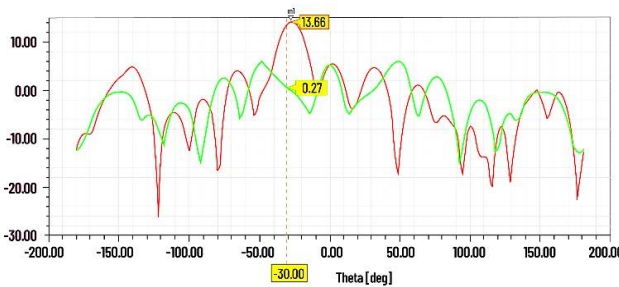


Fig. 17. Results of beam Rotation in the Initial State with. $\theta_{str} = -30^\circ$ and $\varphi_{str} = 0^\circ$ for Case One

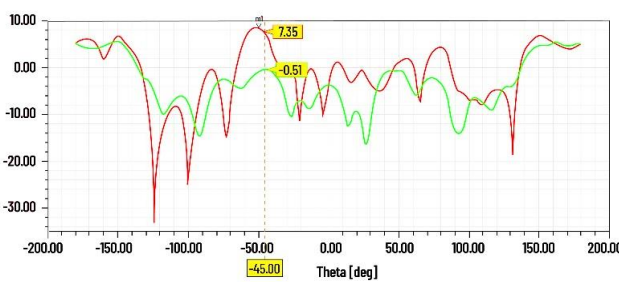


Fig. 18. Results of beam Rotation in the Initial State with. $\theta_{str} = -45^\circ$ and $\varphi_{str} = 0^\circ$ for Case One

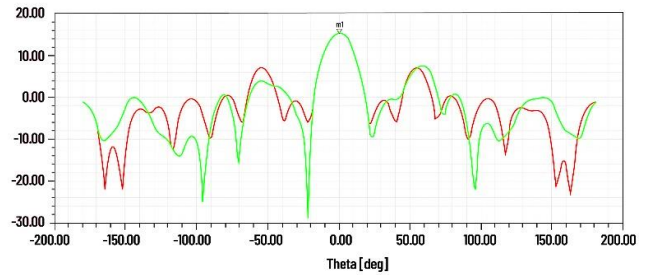


Fig. 19. Results of beam Rotation in the Second State with. $\theta_{str} = 0^\circ$ and $\varphi_{str} = 0^\circ$

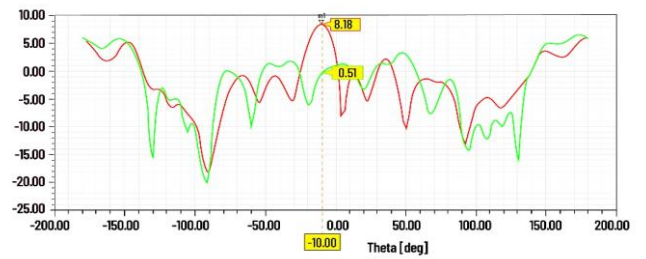


Fig. 20. Results of beam Rotation in the Second State with. $\theta_{str} = -10^\circ$ and $\varphi_{str} = 0^\circ$

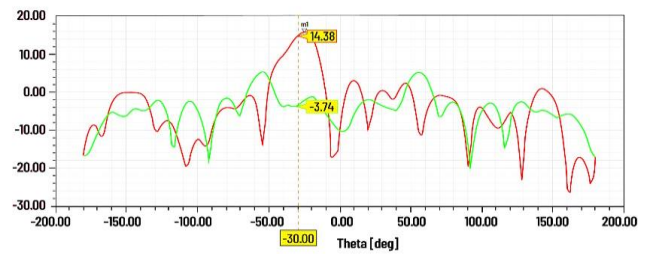


Fig. 21. Results of beam Rotation in the Second State with. $\theta_{str} = -30^\circ$ and $\varphi_{str} = 0^\circ$

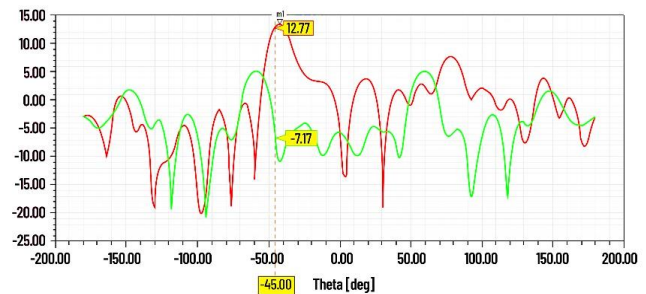


Fig. 22. Results of beam Rotation in the Second State with. $\theta_{str} = -45^\circ$ and $\varphi_{str} = 0^\circ$

D. Beam Steering in the Third State.

In this case, the arrangement of the elements is based on Equation (14,15).

$$\text{for } \begin{cases} 0^\circ \leq \theta_{str} < 30^\circ \\ 0^\circ \leq \varphi_{str} < 30^\circ \end{cases} \begin{cases} 0^\circ < \phi_{total} < 180^\circ \Rightarrow \phi_{total} = 0^\circ \\ 180^\circ \leq \phi_{total} \leq 360^\circ \Rightarrow \phi_{total} = 180^\circ \end{cases} (14);$$

$$\text{for } \begin{cases} 30^\circ \leq \theta_{str} \leq 45^\circ \\ 30^\circ \leq \varphi_{str} \leq 45^\circ \end{cases} \begin{cases} 0^\circ \leq \phi_{total} < 90^\circ \Rightarrow \phi_{total} = 0^\circ \\ 90^\circ \leq \phi_{total} \leq 270^\circ \Rightarrow \phi_{total} = 180^\circ \\ 270^\circ < \phi_{total} \leq 360^\circ \Rightarrow \phi_{total} = 0^\circ \end{cases} (15);$$

The outputs are represented in the following Figs.

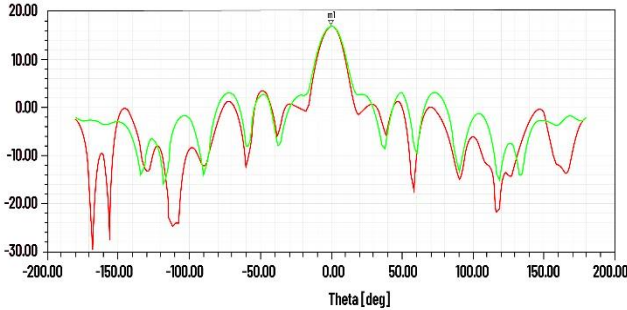


Fig. 23. Results of beam Rotation in the third State with. $\theta_{str} = 0^\circ$ and $\varphi_{str} = 0^\circ$ for Case One

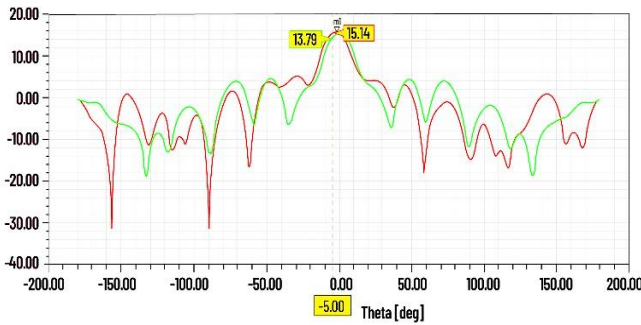


Fig. 24. Results of beam Rotation in the third State with. $\theta_{str} = -5^\circ$ and $\varphi_{str} = 0^\circ$

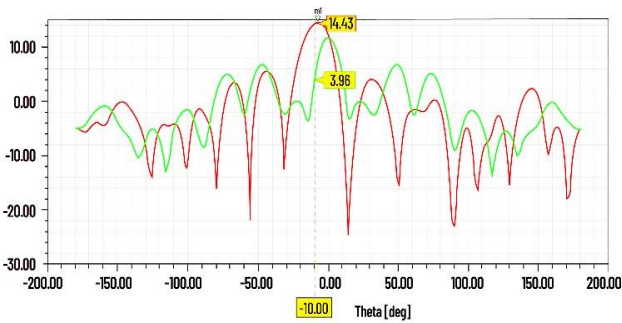


Fig. 25. Results of beam Rotation in the third State with. $\theta_{str} = -10^\circ$ and $\varphi_{str} = 0^\circ$

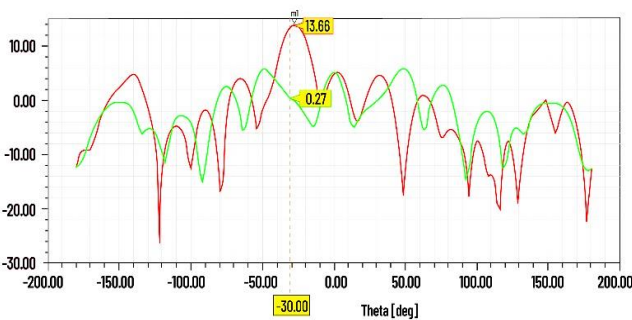


Fig. 26. Results of beam Rotation in the third State with. $\theta_{str} = -30^\circ$ and $\varphi_{str} = 0^\circ$

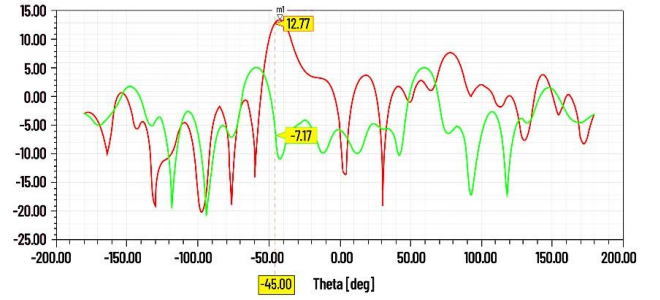


Fig. 27. Results of beam Rotation in the third State with. $\theta_{str} = -45^\circ$ and $\varphi_{str} = 0^\circ$

VI. DISCUSSION

The significant findings of this research are compared with those of previous studies.

First Conclusion: Equation 12 is used for angles greater than 30 degrees, leading to a severe drop in gain. Additionally, Equation 13 is used for angles less than 30 degrees, disrupting the gain balance. For example, the gain at a 30-degree angle is higher than at a 10-degree angle. The proposed method in this study addresses the issues of severe drop and gain imbalance.

Second Conclusion: Using the proposed method at the center frequency of 9.5 GHz, the side lobe level in the single-bit unit cell reaches -17.6 dB. Given this side lobe level, the half-power beam width for the single-bit unit cell is 14.59°, which is one of the requirements of this paper.

VII. BEAM STEERING

This paper examined three cases of beam steering. In this section, the results of the proposed case are compared with the other two cases, and the comparison results are presented in Table II.

VIII. COMPARISON OF THE RESULTS OF THE PROPOSED MODE WITH ANOTHER 2 MODES

The advantage of the unit cell of this design over the two articles 10.1109/LAWP.2018.2817363[17] and "10.1049/iet-map.2018.5288[18]"

Table II
Comparison of Gain Loss in Rotation Angles

third	second,	First	mode
16.5dB	15.1dB	16.5dB	Gain
14.43dB	8.18dB	14.43dB	0°
13.66dB	14.38dB	13.66dB	$\pm 10^\circ$
12.77dB	12.77dB	7.36dB	$\pm 30^\circ$
3.73dB	6.92dB	9.14dB	$\pm 45^\circ$
			The amount of gain loss in rotation angles

First: These two articles are used on circular polarization, while my unit cell is for linear polarization, and these two submitted articles are not suitable for linear polarizations at all

Second: The unit cell of these two submitted articles is multilayered. For example, the article unit cell with flexible transmission phase slope for ultra-wideband transmit array antenna is 4 layers, which naturally

makes its manufacturing cost and manufacturing method much heavier than my unit cell.

Third, in my unit cell, the gain drop is not severe at all.

Fourth: The dimensions of my proposed cell are much smaller than the dimensions of these 2 submitted articles, and because of these large dimensions, it can be problematic in radar applications.

IX. REFERENCES

- [1] D. Liao, Y. Zhang, and H. Wang, "Wide-Angle Frequency-Controlled Beam-Scanning Antenna Fed by Standing Wave Based on the Cutoff Characteristics of Spoof Surface Plasmon Polaritons," *IEEE Antennas Wirel. Propag. Lett.*, vol. 17, no. 7, pp. 1238–1241, 2018, doi: 10.1109/LAWP.2018.2841006.
- [2] J. Abraham and T. Mathew, "A novel dual-band microstrip patch array," *2015 IEEE Appl. Electromagn. Conf. AEMC 2015*, pp. 6–7, 2016, doi: 10.1109/AEMC.2015.7509235.
- [3] L. Di Palma, "1-bit reconfigurable unit-cell based on PIN diodes for," 2016.
- [4] P. F. McManamon *et al.*, "Optical phased array technology," *Proc. IEEE*, vol. 84, no. 2, pp. 268–298, Feb. 1996, doi: 10.1109/5.482231.
- [5] P. McManamon, "An overview of optical phased array technology and status," in *Proc. SPIE*, T. R. Wolinski, M. Warengem, and S.-T. Wu, Eds., Sep. 2005, p. 59470I. Doi: 10.1117/12.631412.
- [6] H. Kamoda, T. Iwasaki, J. Tsumochi, T. Kuki, and O. Hashimoto, "60-GHz Electronically Reconfigurable Large Reflectarray Using Single-Bit Phase Shifters," *IEEE Trans. Antennas Propag.*, vol. 59, no. 7, pp. 2524–2531, Jul. 2011, doi: 10.1109/TAP.2011.2152338.
- [7] A. Yaacobi, J. Sun, M. Moresco, G. Leake, D. Coolbaugh, and M. R. Watts, "Integrated phased array for wide-angle beam steering," *Opt. Lett.*, vol. 39, no. 15, p. 4575, Aug. 2014, doi: 10.1364/OL.39.004575.
- [8] A. Clemente, L. Dussot, R. Sauleau, P. Potier, and P. Pouliguen, "Spatially Sparse Precoding in Millimeter Wave MIMO Systems. IEEE Transactions on Wireless Communications," *IEEE Trans. Antennas Propag.*, vol. 60, no. 5, pp. 2260–2269, May 2012, doi: 10.1109/TAP.2012.2189716.
- [9] F. Sboui, L. Latrach, and A. Gharsallah, "Design of SIW Frequency Agile Antenna Based on a Varactor Loaded on U-Slot," *Mediterr. Microw. Symp.*, vol. 2018-October, pp. 54–56, 2018, doi: 10.1109/MMS.2018.8611792.
- [10] O. Manoochehri, D. Erricolo, A. Darvazehban, and F. Monticone, "Design of compact beam-steering active slot antennas with a metasurface reflector," *2019 United States Natl. Comm. URSI Natl. Radio Sci. Meet. Usn. NRSM 2019*, pp. 1–2, 2019, doi: 10.23919/USNC-URSI-NRSM.2019.8712996.
- [11] W. Li and Y. Zhao, "A pattern reconfigurable patch antenna for wide-angle scanning phased array," *2016 IEEE/ACES Int. Conf. Wirel. Inf. Technol. ICWITS 2016 Syst. Appl. Comput. Electromagn. ACES 2016 - Proc.*, pp. 3–4, 2016, doi: 10.1109/ROPACES.2016.7465428.
- [12] O. El Ayach, S. Rajagopal, S. Abu-Surra, Z. Pi, and R. W. Heath, "10-GHz Low-Loss Liquid Metal SIW Phase Shifter for Phased Array Antenna," *IEEE Trans. Wirel. Commun.*, vol. 13, no. 3, pp. 1499–1513, Mar. 2014, doi: 10.1109/TWC.2014.011714.130846.
- [13] S. Alkaraki *et al.*, "10-GHz Low-Loss Liquid Metal SIW Phase Shifter for Phased Array Antennas," *IEEE Trans. Microw. Theory Tech.*, vol. 71, no. 11, pp. 5045–5059, Nov. 2023, doi: 10.1109/TMTT.2023.3308160.
- [14] A. Clemente *et al.*, "Reconfigurable transmitarray antennas at," 2022.
- [15] L. Vinet and A. Zhedanov, "A 'missing' family of classical orthogonal polynomials," *J. Phys. A Math. Theor.*, vol. 44, no. 8, p. 085201, Feb. 2011, doi: 10.1088/1751-8113/44/8/085201.
- [16] C. A. Balanis, *Handbook, Modern Antenna*. 2008.
- [17] S. H. Ramazannia Tuloti, P. Rezaei, and F. Tavakkol Hamedani, "High-Efficient Wideband Transmitarray Antenna," *IEEE Antennas Wirel. Propag. Lett.*, vol. PP, p. 1, Mar. 2018, doi: 10.1109/LAWP.2018.2817363.
- [18] R. T. S.H., R. P., and T. H. F., "Unit cell with flexible transmission phase slope for ultra-wideband transmitarray antennas," *IET Microwaves, Antennas Propag.*, vol. 13, no. 10, pp. 1522–1528, Aug. 2019, doi: 10.1049/iet-map.2018.5288.